Composites Science and Technology 87 (2013) 69–76

Contents lists available at ScienceDirect

Composites Science and Technology

journal homepage: www.elsevier.com/locate/compscitech

Interfacial reaction and nanostructures in Mg matrix composites reinforced with carbon fibers modified by sol–gel method

W.G. Wang [a,b], B.L. Xiao [a], Z.Y. Ma [a,*]

[a] Shenyang National Laboratory for Materials Science, Institute of Metal Research, Chinese Academy of Sciences, 72 Wenhua Road, Shenyang 110016, China
[b] Liaoning Shihua University, 1 Dandong Road, Fushun 113001, China

ARTICLE INFO

Article history:
Received 12 March 2013
Received in revised form 27 July 2013
Accepted 30 July 2013
Available online 7 August 2013

Keywords:
A. Metal matrix composites (MMCs)
A. Carbon fibers (C_f)
E. Sol–gel methods
B. Interfaces

ABSTRACT

Continuous carbon fibers (C_f) were modified with γ-Al_2O_3 and anatase-TiO_2 coatings in sol–gel route, and used to prepare 45 vol.% C_f reinforced Mg matrix composites (referred to as Al_2O_3–C_f and TiO_2–C_f composites) using a vacuum pressureless infiltration process, producing the tensile strengths of 550 MPa and 980 MPa, respectively. During the composite fabrication, the Mg matrix reacted with the coatings to form the interfacial layers composed primarily of MgO nanoparticles, with a size of about 10–20 nm and 3–5 nm, respectively, for the Al_2O_3–C_f and TiO_2–C_f composites. Such interfacial reaction produced a volume expansion in the interfacial layer, resulting in the formation of a great deal of crystal defects, such as distorted lattice, dislocation and amorphous intergranular phase. The Al_2O_3–C_f composite exhibited lower tensile strength due to greater volume expansion in the interfacial layer. A few TiC and TiO_2 nanoparticles were observed in the interfacial layer of the TiO_2–C_f composite. This is attributed to the restraining effect of the reduced Ti accumulated in the near-interface matrix on the atom diffusion (Mg and Ti), remaining some TiO_2 nanoparticles at the surface of C_f. This showed a new self-regulating mechanism of interfacial reaction.

1. Introduction

Continuous carbon fiber (C_f) exhibits high tensile strength and high modulus with low density, and is an ideal reinforcement for metal matrix composites (MMCs) [1–4]. Since the wetting between C_f and metal matrix is poor and C_f can react with many metal elements in the processes of fabricating the C_f reinforced MMCs (CfMMCs), the interface compatibility problem between C_f and metal matrix limits the strength improvement of CfMMCs [4–8]. In order to take advantage of the superior properties of C_f fully, an interfacial optimization design is necessary [6–12].

Many studies [6–12] have been carried out to overcome the interface compatibility problem. Among them, to modify the surface of C_f using coating was recognized as an effective and practical method. Surface coating processes include chemical vapor deposition (CVD) [11], electro [13] and electroless [7] plating, molten salt [14,15], sol–gel [9,16–18] and so on. Among these methods, the sol–gel method has attracted much attention due to its distinct advantages, such as low cost, simple routine, and low equipment requirement. Moreover, controllability of the nanostructured sol–gel coating is very attractive since it provides a shortcut to study the unusual deformation mechanisms of nanocrystalline interfacial layers in CfMMCs as well as an important approach to design and control the interfacial nanostructure and interfacial reaction precisely.

Chen and Li [18] modified the surface of C_f (M40, made by Japanese Toray company) with SiO_2 coating, and produced 40 vol.% C_f reinforced ZM5 Mg matrix composite with a tensile strength of 663 MPa. Wu et al. [10] fabricated 55 vol.% SiC coated C_f reinforced AZ81 Mg matrix composite, and obtained a tensile strength of 1038 MPa, about 70% of the theoretical value. In our recent report, the tensile strength of 45 vol.% C_f reinforced Mg matrix composite could reach 1.08 GPa (90% of the theoretical prediction) through interface coating design using yttria stabilized zirconia (YSZ) sol–gel [9]. Although the fabrication routes of the above CfMMCs were similar (liquid infiltration), the mechanical properties of these CfMMCs were quite different. Specially, the ratio of the experimentally measured strength to the predicted strength by the rule of mixture showed a great difference. The interfacial microstructure could be considered as the primary factor, since the interface plays an important role in the load transfer between reinforcement and matrix [8–12,19–21].

Generally, there was an interfacial layer between metal matrix and C_f in CfMMCs due to the coatings of C_f and the interfacial reaction, with the coatings being tens to hundreds of nanometers thick and composed of nanocrystalline [9–11,16–18]. It is expected that the performances of CfMMCs could be further improved based on

* Corresponding author. Tel./fax: +86 24 83978908.
E-mail address: zyma@imr.ac.cn (Z.Y. Ma).

0266-3538/$ - see front matter © 2013 Elsevier Ltd. All rights reserved.
http://dx.doi.org/10.1016/j.compscitech.2013.07.027

the excellent properties of nanomaterials. Therefore, it is necessary to study the microstructures of the interfacial layers at the nanoscale. Unfortunately, it is very difficult to observe the intragranular or intergranular nanostructures of interfacial layers even using high-resolution transmission electron microscopy (HRTEM). As a result, the report on the interfacial nanostructure was few.

In order to clarify the inherent relationship between interfacial reaction and interfacial nanostructures, it is necessary to prepare some model CfMMCs with the same or similar thickness and chemical compositions of interfacial layers. In our recent study, nanostructured coating based on yttria stabilized zirconia (YSZ) sol–gel was used to prepare to 45 vol.% C_f/Mg composite, producing a tensile strength of 90% theoretical prediction [9]. It is interesting to examine whether other coatings would achieve the same performance.

In this study, the C_f was modified with γ-Al_2O_3 and anatase-TiO_2 coatings, respectively, in sol–gel route, and 45 vol.% C_f/Mg composites were fabricated using a vacuum pressureless infiltration process. The aim is to investigate the interface reaction mechanism and interfacial nanostructures with these coatings and to understand the inherent relationships among interfacial reaction, interfacial nanostructures and mechanical properties of CfMMCs further.

2. Material and methods

2.1. Preparation of C_f preforms

Unidirectionally aligned high strength carbon fibers (PAN, made in China) with a diameter of 7 μm were used in this study. The preforms of $60 \times 25 \times 5$ mm^3 containing about 45 vol.% C_f were prepared by a filament winding technique. In order to remove the sizing agent on the surfaces of C_f, the preforms were heated at 450 °C for 30 min in a vacuum furnace (5×10^{-2} Pa). After removing the sizing agent, the tensile tests of C_f with a gauge length of 15 mm were conducted at an initial strain rate of 5×10^{-3} s^{-1} on a Hounsfield H5K-S electronic testing machine. 30 specimens were tested and the average tensile strength of C_f was determined to be 2.6 GPa, according to the ASTM D3379-75 standard [22].

2.2. Preparation of sol–gel coating

In this experiment, all the chemicals were analytical reagent and made by Sinopharm Chemical Reagent Co., Ltd.

AlOOH sol was prepared using aluminum isopropoxide ($Al(C_3$-$H_7O)_3$) as a precursor. Firstly, the deionized water was heated up to 80–90 ° C, and then the $Al(C_3H_7O)_3$ was dissolved in deionized water with a molar concentration of 0.2 mol/l. Under magnetic stirring, monohydrate alumina precipitate was formed by hydrolysis, i.e. boehmite precipitation. Dripping aqueous solution of nitric acid as the peptizer, the pH value was adjusted to 3.0–3.5. In order to distill the isopropanol off from the sol, the sol was heated to 90 °C for 1 h. Finally, the reaction vessel was closed and maintained for 24 h at 80 °C to get clear γ-AlOOH sol.

In addition, using tetrabutyl titanate ($Ti(OC_4H_9)_4$) as a precursor, anhydrous ethanol as a solvent, acetylacetone as a chelating agent, nitric acid as an inhibitor, TiO_2 sol was prepared. The volume ratio of tetrabutyl titanate, anhydrous ethanol, deionized water, and acetylacetone was 1:9:0.7:0.15. Firstly, deionized water and 1/3 of anhydrous ethanol were mixed, and the pH value of solution was adjusted to 3.0 with nitric acid. The obtained solution was denoted by solution A. Tetrabutyl titanate and acetylacetone were added into 2/3 of anhydrous ethanol, and solution B was obtained. Under magnetic stirring, solution A was slowly instilled into solution B to obtain a uniform and transparent sol.

The C_f preforms were immerged in the obtained sols and ultrasonically vibrated for 10 min, and then removed from the sols and dried in the shade. The sintering of C_f preforms was carried out at 735°C for 60 min in a vacuum furnace (5×10^{-2} Pa).

In order to identify the crystalline phase of coatings, Al_2O_3 and TiO_2 powders were prepared through drying the Al_2O_3 and TiO_2 sol at room temperature. Consistent with the sintering of C_f preforms, Al_2O_3 and TiO_2 powders were sintered at 735°C for 60 min in a vacuum furnace (5×10^{-2} Pa). And then, these powders were analyzed using the X-ray diffraction (XRD) technique on a D/max 2500PC diffractometer using Cu Ka radiation.

2.3. Fabrication of C_f/Mg composite

A commercial pure Mg matrix composite reinforced with 45 vol.% C_f was fabricated using a pressureless infiltration process in vacuum. As the first step, Mg ingots and C_f preforms were sealed in a steel die. Then they were heated in a vacuum furnace to 750°C, and the temperature was maintained for 30 min in order to carry out the liquid metal infiltration. After the infiltration, the CfMMCs were cooled down directly in the vacuum furnace. The 45 vol.% C_f/Mg matrix composites with Al_2O_3 and TiO_2 coatings were denoted by Al_2O_3–C_f and TiO_2–C_f composites, respectively.

2.4. Characterization

The microstructures of the Al_2O_3–C_f and TiO_2–C_f composites were examined using scanning electron microscopy (SEM, Nova NanoSEM 430) and transmission electron microscopy (TEM, FEI Tecnai F20). Thin foils for TEM were prepared by the ion milling technique.

Tensile specimens of CfMMCs with a gauge length of 10.0 mm, a width of 2.0 mm and a thickness of 1.5 mm were machined from CfMMCs parallel to the longitudinal direction of C_f. Tensile tests were conducted at room temperature and an initial strain rate of 3.3×10^{-4} s^{-1} on a Zwick/Roell Z050 tester.

3. Results

3.1. The characteristics of coatings

Fig. 1(a) shows the coarse surfaces of unsized C_f. After calcination at 735°C for 60 min in vacuum, both Al_2O_3 and TiO_2 coatings could be coated on the surfaces of C_f and the coatings were uniform and smooth, as shown in Fig. 1(b and c), respectively. In addition, neither crinkle nor crack was found on the two coatings. This indicates that both Al_2O_3 and TiO_2 coatings were formed on the C_f surfaces very well.

Fig. 2 shows the XRD patterns of Al_2O_3 and TiO_2 powders prepared with sol–gel method and sintered at 735°C for 60 min. It was indicated that the crystalline phase was γ-Al_2O_3 and anatase-TiO_2, respectively. Since the fabricating processing of powders was the same as that of Al_2O_3 and TiO_2 coatings on C_f, it is believed that the coating on the surfaces of C_f was γ-Al_2O_3 and anatase-TiO_2, respectively.

3.2. The tensile properties and microstructures of CfMMCs

The tensile strength of Al_2O_3–C_f and TiO_2–C_f composites was determined to be 550 MPa and 980 MPa, respectively. Clearly, although the fabrication processes were almost same, the tensile properties of Al_2O_3–C_f and TiO_2–C_f composites showed a large difference. This implies that interfacial nanostructure played a primary role.

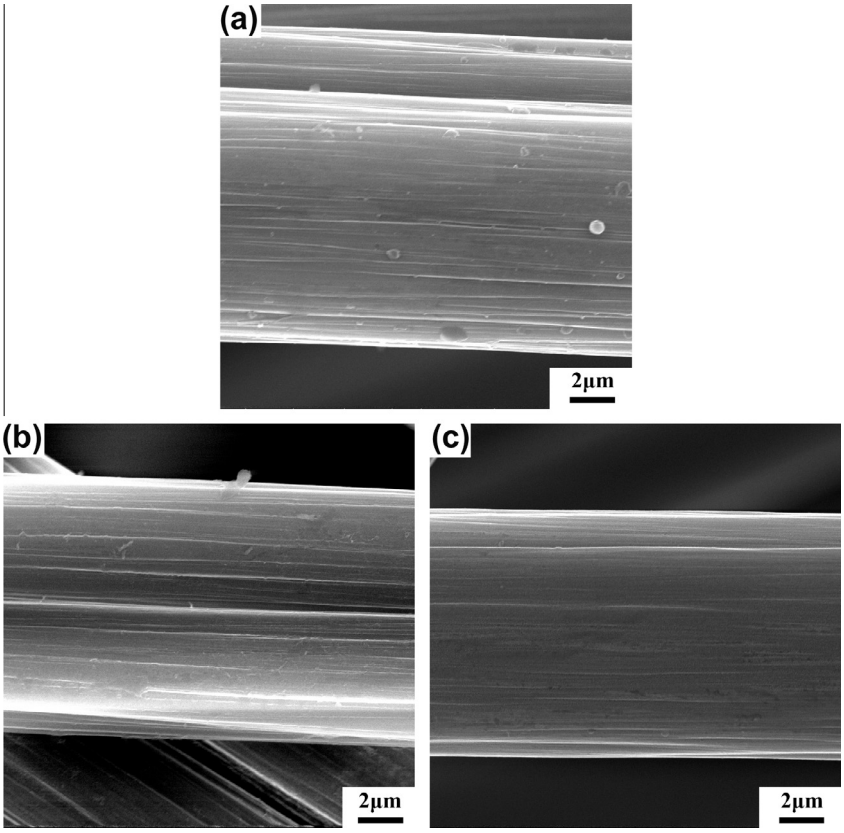

Fig. 1. SEM images of (a) unsized, (b) Al_2O_3 and (c) TiO_2 sol coated C_f after calcination at 735 °C for 60 min, respectively.

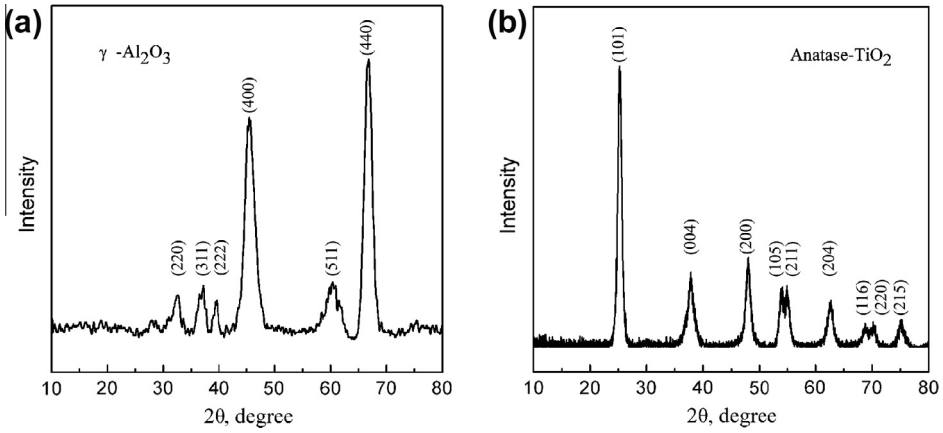

Fig. 2. XRD patterns of (a) γ-Al_2O_3 and (b) anatase-TiO_2 powders prepared with sol–gel method and sintered at 735 °C for 60 min, respectively.

Fig. 3(a and c) show the cross-sectional SEM micrographs of Al_2O_3–C_f and TiO_2–C_f composites, respectively. The molten Mg infiltrated completely the interspaces among the C_f without a pressure as infiltrating force. It indicates that both coatings could improve the wetting between the C_f and the Mg matrix greatly. The interfacial bonding between the C_f and the Mg matrix was very good without discernible debonding or micro-crack. Moreover, the distributions of C_f were uniform and no obvious difference could be found between Al_2O_3–C_f and TiO_2–C_f (Fig. 3(b–d)) composites. However, some bright lines could be observed around C_f in the TiO_2–C_f composite (Fig. 3(d)). According to the EDS analysis, the bright line was determined to be the Mg matrix with relatively high concentration of Ti. Although the contrast was very clear, the concentration of Ti was less than 1.0 at.% since TiO_2 coating was very thin. Obviously, with the prolonging of infiltrating time, the bright line would disappear gradually.

3.3. The interfacial nanostructures

Fig. 4 shows the TEM microstructures of the interfaces in the Al_2O_3–C_f and TiO_2–C_f composites. It can be seen that the surfaces of the C_f are wrapped with a thin and uniform interfacial layer with a thickness of nanoscale. No obvious difference could be found between the interfacial layers of Al_2O_3–C_f and TiO_2–C_f composites at submicron scale.

Fig. 5(a) shows the high resolution TEM (HRTEM) image of the interfacial layer in the Al_2O_3–C_f composite, and the thickness of interfacial layer was 15–20 nm. Fig. 5(b) shows the magnified

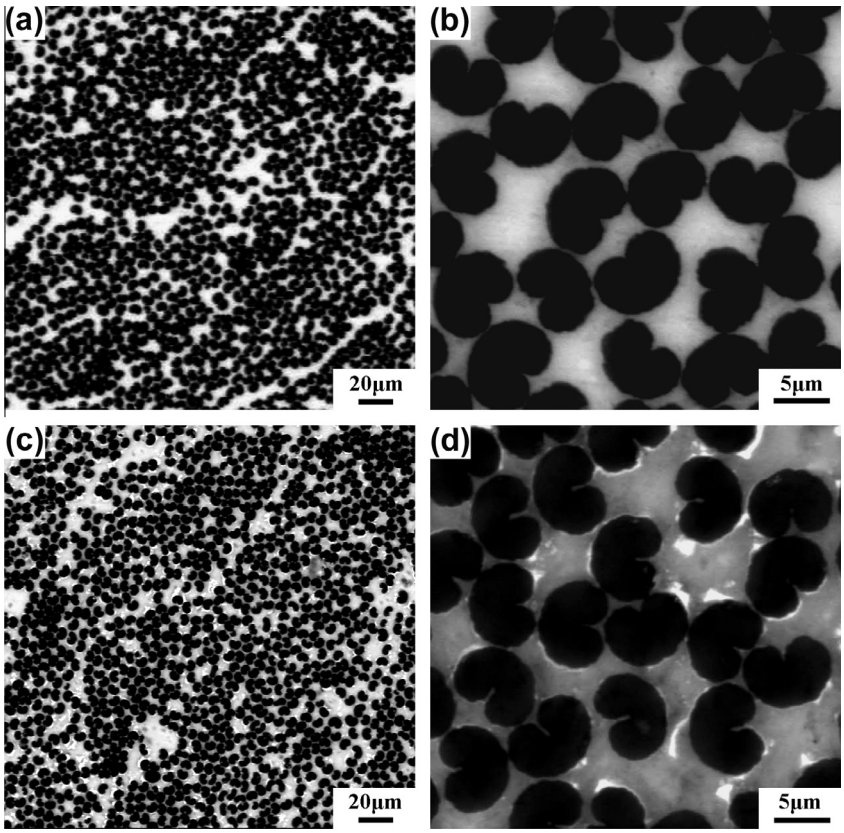

Fig. 3. SEM micrographs of Al_2O_3–C_f composite under (a) low and (b) high magnification, and TiO_2–C_f composite under (c) low and (d) high magnification.

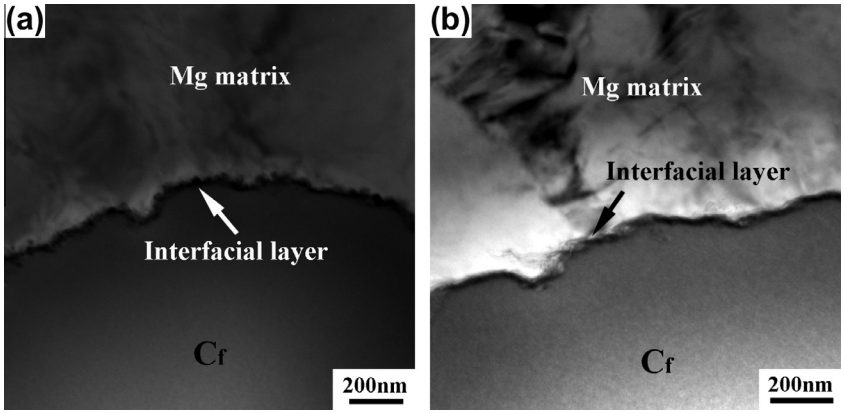

Fig. 4. TEM images showing interfacial microstructure in (a) Al_2O_3–C_f composite and (b) TiO_2–C_f composite.

image of region B framed with black lines in Fig. 5(a). It was proved that the interfacial layer was composed of MgO nano-particles and the interfacial reaction should obey following chemical equation:

$$Al_2O_3 + 3Mg \rightarrow 2Al + 3MgO \quad (1)$$

HRTEM image showed that the size of MgO particles was 10–20 nm and similar with the thickness of the interfacial layer. According to the Fast Fourier Transform (FFT) image shown at the upper right corner of Fig. 5(a) and HRTEM image of Fig. 5(b), an orientation relationship between MgO nano-particles and Mg matrix was found: $(1\bar{1}1)_{Mg}//(\bar{1}11)_{MgO}$ and $[231]_{Mg}//[110]_{MgO}$. The mismatch between the $(1\bar{1}1)_{Mg}$ plane spacing of Mg (0.245 nm) and $\bar{1}11_{MgO}$ plane spacing of MgO (0.243 nm) was about 0.82%.

Moreover, some crystal defects could be found in the interfacial layer of the Al_2O_3–C_f composite. Fig. 6(a) shows that the interfacial nanostructures were ubiquitous in the Al_2O_3–C_f composite. An amorphous intergranular film could be observed in the interfacial layer. Fig. 6(b) is the magnified image of region B framed with white lines in Fig. 6(a), and a black straight line was drawn in Fig. 6(b) in order to form a contrast with the distorted MgO lattice. The crystal defects were so severe that some arc-like MgO lattice could be observed easily. It should be emphasized that neither remaining Al_2O_3 particle nor interfacial reaction product Al_4C_3 was found at the interface.

Similarly, the interfacial nanostructure in the TiO_2–C_f composite was observed as well. Fig. 7(a) shows that the surface of C_f was covered completely with a uniform interfacial layer with a

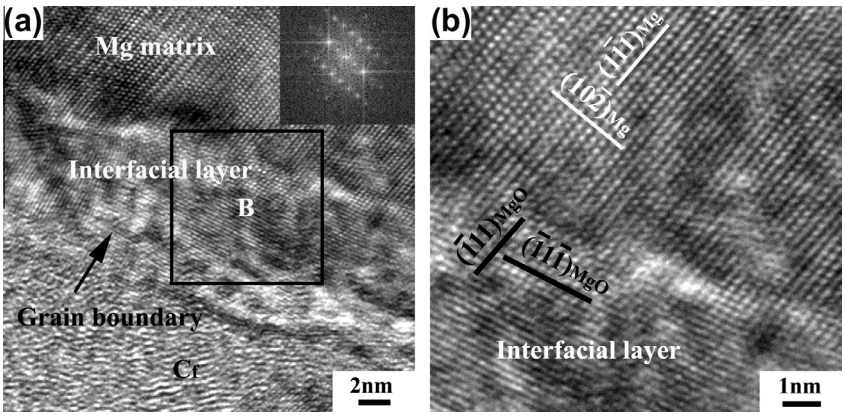

Fig. 5. (a) HRTEM image of interfacial layer in Al_2O_3–C_f composite, (b) magnified image of regions B in (a).

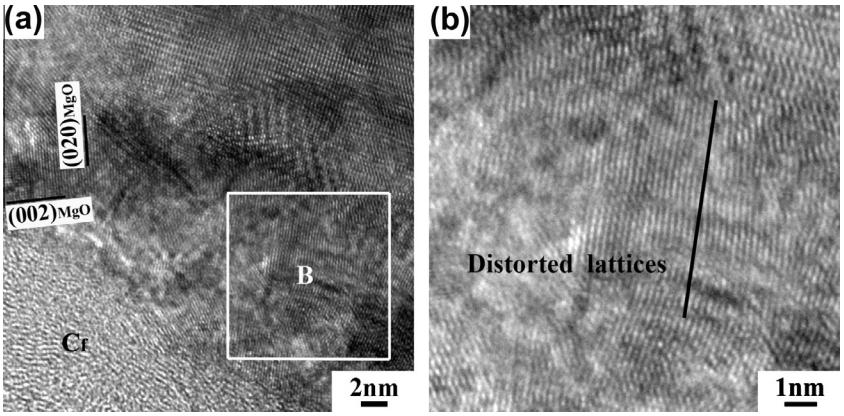

Fig. 6. (a) HRTEM image of interfacial layer in Al_2O_3–C_f composite, and (b) magnified image of region B framed in (a).

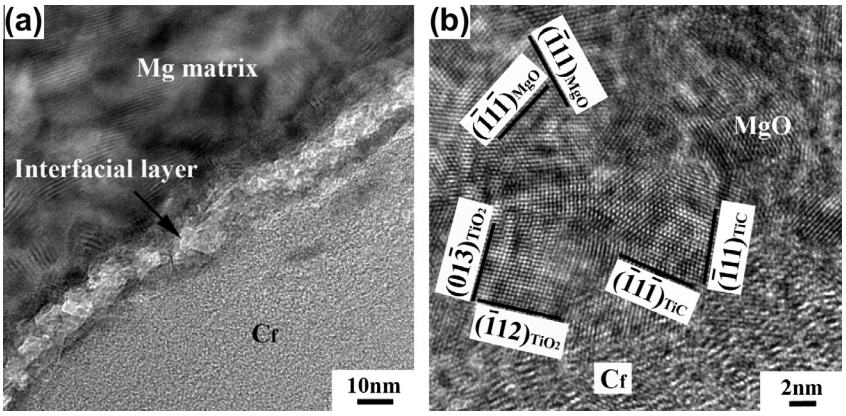

Fig. 7. (a) HRTEM image of interfacial layer in TiO_2–C_f composite, and (b) magnified image.

thickness of 15–20 nm. Fig. 7(b) clearly shows that the interfacial layer consisted of tiny MgO, TiC and remaining TiO_2 particles. MgO was the primary component of the interfacial layer, and no orientation relationship was found among these nano-particles. The remaining TiO_2 particles existed on the surface of C_f and were covered with MgO particles, and the crystalline phase of remaining TiO_2 was still anatase. This indicates that some factors played a good barrier role for restraining the interfacial reaction between the Mg matrix and the TiO_2 particles. Moreover, a small amount of TiC could be found near the surface of C_f. The interfacial reactions should obey following chemical equations:

$$TiO_2 + 2Mg \rightarrow Ti + 2MgO \quad (2)$$

$$Ti + C \rightarrow TiC \quad (3)$$

Fig. 8(a) shows that the interfacial layer was composed of about 5 layers of nanoparticles with the grain size of about 3–5 nm. Fig. 8(b and c) shows the nanostructure of grain boundaries B and C marked in Fig. 8(a). Grain boundaries B and C were close to the Mg matrix and C_f, respectively. The closer to the Mg matrix, the thicker the amorphous intergranular film is. Moreover, the edge dislocation could be found in the MgO nano-particles, as shown in Fig. 8(d).

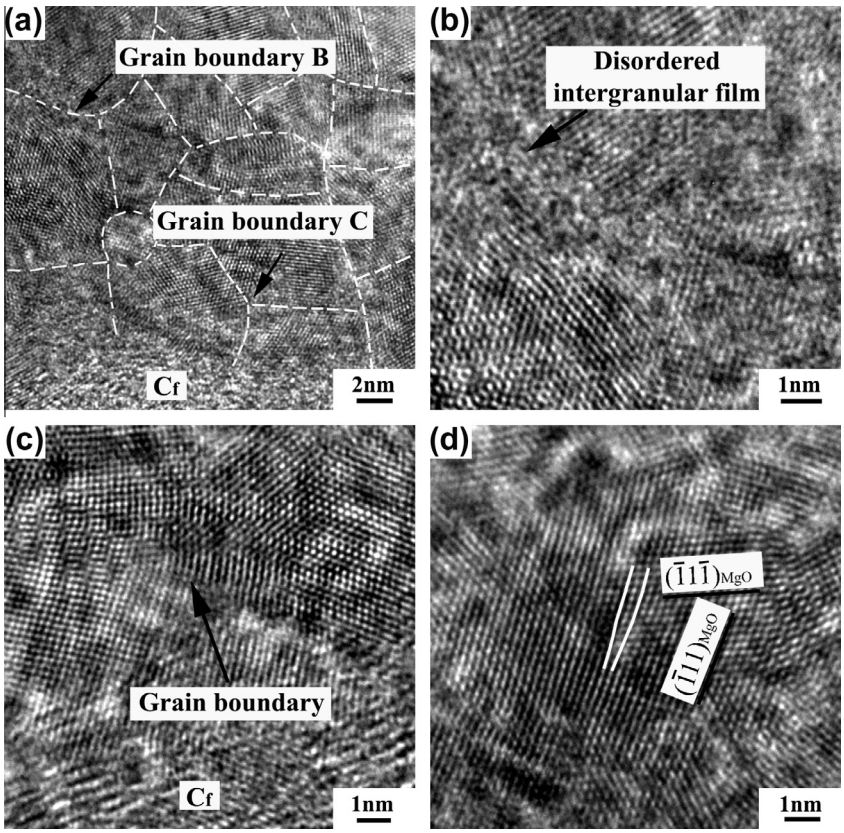

Fig. 8. (a) HRTEM image of interfacial layer in TiO_2–C_f composite; (b) and (c) magnified image of region B and C in (a), respectively; (d) magnified image of intragrain in (a).

4. Discussion

4.1. The effects of interfacial reaction on interfacial nanostructure

According to above HRTEM observation (Figs. 5–8), the interfacial layers showed different nanostructures in the Al_2O_3–C_f and TiO_2–C_f composites. In the Al_2O_3–C_f composite, the interfacial layer was completely composed of MgO nano-particles, and the lattice of MgO was distorted into arc-like (Fig. 6(b)). In the TiO_2–C_f composite, the interfacial layer could be divided into outside (near the Mg matrix) and inside (near the C_f) layers according to the chemical compositions. In the outside layer, MgO was the primary component; in the inside layer, not only TiO_2 remained, but also a small quantity of TiC were formed. The edge dislocations could be found in the MgO nano-particles (Fig. 8(d)), but the degree of crystal defects was less than that in the Al_2O_3–C_f composite. Moreover, in the TiO_2–C_f composite, the amorphous intergranular films could be observed in the outside interfacial layer, and the thickness was about 1 nm (Fig. 8(b)). Nevertheless, the amorphous intergranular films almost could not be found in the inside interfacial layer. It was evident that there was an inherent relationship between interfacial reaction and interfacial crystal defects, namely the more exhaustive interfacial reaction is, the larger the volume expansion is and the severer the interfacial crystal defects are.

In this study, all the C_f performs were sintered at 735 °C for 60 min before infiltration process. In order to identify the crystalline phase of coatings, Al_2O_3 and TiO_2 powders, prepared using the same route as that for the coatings in C_f preforms, were subjected to XRD analyses. It was revealed that the crystalline phase of powders was γ-Al_2O_3 and anatase-TiO_2, respectively (Fig. 2). This indicates that the crystalline phase of original coatings on the surfaces of C_f should be γ-Al_2O_3 and anatase-TiO_2, respectively. This result is consistent with HRTEM observations (Fig. 7) and the previous studies [16].

According to Eqs. (1) and (2), 1 mol of Al_2O_3 and TiO_2 would form 3 and 2 mol of MgO, respectively. Since the majority of the deoxidized Al and Ti were dissolved into the molten Mg matrix, the volume change caused by the interfacial reaction could be calculated, as listed in Table 1. It should be pointed out that though the Ti would react with C_f to form TiC, the volume of TiC could be neglected due to the little quantity. The calculation result reveals that the interfacial reaction would result in the volume expansion of interfacial layer and the volume expansion rate of γ-Al_2O_3 coating was almost 3 times of that of TiO_2 coating.

With the progressing of interfacial reaction, a large compressive stress could be induced, and the volume expansion rate of interfacial layer would exceed greatly the range of elastic deformation of brittle ceramics. According to the previous studies [23–25], brittle nanocrystalline ceramics exhibited unusual deformation mechanisms resulting from the coexistence of brittle grains and soft amorphous grain boundary (GB) phases. The crossover from intergranular deformation to intragranular deformation has been simulated [25]. These studies verified that the crossover arises from the interplay between cooperative grain sliding, grain rotations, and intergranular dislocation formation similar to stick–slip behavior. Therefore, under a large compressive stress field caused by the interfacial reaction, the amorphous intergranular film and intragrain crystal defects could be considered as the evidence of unusual deformation in the interfacial layer.

It should be pointed out that the thickness distribution of amorphous intergranular film was different in the interfacial layer of the TiO_2–C_f composite, as shown in Fig. 8(b and c). The closer to the Mg

Table 1
Volume change caused by interfacial reaction between γ-Al_2O_3 and anatase-TiO_2 coatings and Mg matrix.

Reaction equations	$Al_2O_3 + 3Mg \rightarrow 3MgO + 2Al$		$TiO_2 + 2\,Mg \rightarrow 2MgO + 2Ti$	
	1 mol of Al_2O_3	3MgO	1 mol of TiO_2	2MgO
Volume	27.49 cm^3	33.48 cm^3	20.54 cm^3	22.32 cm^3
Rate of volume change	(33.48–27.49 cm^3)/27.49 $cm^3 \approx 21.8\%$		(22.32–20.54cm^3)/20.54 $cm^3 \approx 8.7\%$	

matrix, the thicker the amorphous intergranular film is. This means that the closer to the Mg matrix the severer deformation of nanocrystalline is. Taking account of the diffusion path of Mg and the positions of remaining TiO_2 nano-particles, it is clarified that the closer to the Mg matrix, the more exhaustive interfacial reaction is and the larger the volume expansion is. As a result, in the interfacial layer of the TiO_2–C_f composite, the crystal defects and chemical composition showed a gradient distribution.

4.2. The effects of interfacial nanostructure on the interfacial reaction

Although some TiO_2 nanoparticles could be retained near the surface of C_f in the TiO_2–C_f composite, no remaining Al_2O_3 nanoparticles were found in the Al_2O_3–C_f composite. This phenomenon may be due to the following factors:

(1) In the Al_2O_3–C_f composite, the amorphous intergranular film and intragranular crystal defects of MgO nanoparticles acted as a shortcut of Mg atom migration, and Mg could keep on reacting with Al_2O_3 coating.
(2) In the TiO_2–C_f composite, Ti is the deoxidized product of interfacial reaction. According to the previous study [26], the mixture enthalpy (ΔH^{Mix}_{A-B}) of the binary liquid in Ti–Mg and Al–Mg systems at an equi-atomic composition is 16 kJ/mol and −2 kJ/mol, respectively. Obviously, it is difficult for the deoxidized product Ti to dissolve into molten Mg matrix, though it is very easy for Al. This has been also verified in this study, as shown in Fig. 3(b–d). With the progressing of interfacial reaction, Ti would be accumulated at the matrix near the interface. Obviously, the existence of Ti would decrease the chemical activity of Mg. At the same time, the Ti-rich near-interface matrix could counteract the diffusion of Ti and Mg between the interfacial layer and the Mg matrix. As a result, the TiO_2 nanoparticles were retained and TiC was formed in the TiO_2–C_f composite. On the contrary, in the Al_2O_3–C_f composite, no Al_2O_3 and Al_4C_3 were observed. This is consistent with our recent study [9] that remaining ZrO_2 and ZrC could be found in the interfacial layer of YSZ CfMMC since the mixture enthalpy of Zr–Mg system is 6 kJ/mol [26].

As the products of interfacial reaction, Ti could accumulate to the near-interface matrix, as shown in Fig. 3(d). Since it is difficult to dissolve Ti into the Mg matrix (ΔH^{Mix}_{Ti-Mg} is 16 kJ/mol [26]) and the melting point of Ti is much higher than that of Mg, a solid rich-Ti film would be formed between interfacial layer on C_f and Mg matrix. The solid rich-Ti film could not be moved away by molten Mg matrix and plays the role of restraining the atom diffusion (Mg), in the processing of interfacial reaction. As a result, the interfacial reaction could be restrained and some remained TiO_2 could be found in the interfacial layer, as shown in Fig. 7(b). On the contrary, since it is easy to dissolve Al into molten Mg matrix (ΔH^{Mix}_{Al-Mg} is −2 kJ/mol [26]), the Al_2O_3 was depleted and no remained Al_2O_3 could be found in the Al_2O_3–C_f composite, as shown in Fig. 5. In the present study, the interaction between interfacial reaction product (e.g. Ti) and interfacial reaction is called self-regulating mechanism. It is thought that the self-regulating mechanism has a certain worth to control the interfacial reaction in MMCs.

5. Conclusions

1. Using the sol–gel coating method, an uniform and smooth γ-Al_2O_3 and anatase-TiO_2 coatings were obtained on the surfaces of C_f. The 45 vol.% C_f/Mg composites were successfully fabricated using the pressureless infiltration process in vacuum, producing a tensile strength of 550 MPa and 980 MPa, respectively.
2. MgO nano-particles were the main components of the interfacial layers, since Mg could react with both γ-Al_2O_3 and anatase-TiO_2 coatings. The thickness of the interfacial layers was about 20 nm and the size of MgO particles was 10–20 nm and 3–5 nm, respectively, in the Al_2O_3–C_f and TiO_2–C_f composites.
3. The interfacial reaction led to volume expansion of interfacial layer. The volume expansion rate for the transformation from Al_2O_3 to MgO and from TiO_2 to MgO was about 21.8% and 8.7%, respectively. As a result, some crystal defects were formed in the interfacial layer and became severe as the volume expansion rate increased.
4. In the TiO_2–C_f composite, a small quantity of deoxidized Ti diffused to the surfaces of C_f and reacted with C_f to form tiny TiC particles, and some remaining TiO_2 particles could be observed near the surface of C_f. Nevertheless, neither Al_2O_3 nor Al_4C_3 were detected in the Al_2O_3–C_f composite.
5. A new self-regulating mechanism of interfacial reaction was revealed. Because the product Ti of interfacial reaction was difficult to dissolve into the molten Mg matrix, Ti would accumulate at the matrix near the interface to form a layer with a high concentration of Ti. This layer could counteract the diffusion between the interfacial layer and matrix, thereby inhibiting the interfacial reaction.

Acknowledgements

The authors gratefully acknowledge the support of the National Basic Research Program of China under grant Nos. 2006CB605306 and 2012CB619600 and the China Postdoctoral Science Foundation.

References

[1] Dieter L, Herwig P, Martin M, Christian R, Oskar P. Elastic moduli of nanocrystallites in carbon fibres measured by in situ X-ray microbeam diffraction. Carbon 2003;41:563–70.
[2] Evans A, Marchi CS, Mortensen A. Metal matrix composites in industry: an introduction and a survey. Kluwer Academic Publisher; 2003.
[3] Rawal S. Metal–matrix composites for space applications. JOM 2001;53(4):14–7.
[4] Landry CC, Barron AR. MOCVD of alumina-silica oxidation resistant coatings on carbon fibres. Carbon 1995;33:381–7.
[5] Suzuki T. The compatibility of pitch-based carbon fibres with aluminum for the improvement of aluminum-matrix composites. Compos Sci Technol 1996;56:147–53.
[6] Wang YC, Zhou BL. Behaviour of coatings on reinforcements in some metal matrix composites. Composites Part A 1996;27:1139–45.
[7] Rams J, Urena A, Escalera MD, Sanchez M. Electroless nickel coated short carbon fibres in aluminium matrix composites. Composites Part A 2007;38:566–75.

[8] Rajan TPD, Pillai RM, Pai BC. Reinforcement coatings and interfaces in aluminium metal matrix composites. J Mater Sci 1998;33:3491–503.
[9] Wang WG, Xiao BL, Ma ZY. Evolution of interfacial nanostructures and stress states in Mg matrix composites reinforced with coated continuous carbon fibres. Compos Sci Technol 2012;72:152–8.
[10] Wu F, Zhu J, Chen Y, Zhang G. The effects of processing on the microstructures and properties of Gr/Mg composites. Mater Sci Eng A 2000;277:143–7.
[11] Reischer F, Pippel E, Woltersdorf J, Stockel S, Marx G. Carbon fibre-reinforced magnesium: improvement of bending strength by nanodesign of boron nitride interlayers. Mater Chem Phys 2007;104:83–7.
[12] Clyne TW, Watson MC. Interfacial mechanics in fibre-reinforced metals. Compos Sci Technol 1991;42:25–55.
[13] Gawad OA, Tabl MHA, Hamid ZA, Mostafa SF. Electroplating of chromium and Cr-carbide coating for carbon fibre. Surf Coat Technol 2006;201:1357–62.
[14] Baumli P, Sychev J, Budai I, Szabo JT, Kaptay G. Fabrication of carbon fibre reinforced aluminum matrix composites via a titanium-ion containing flux. Composites Part A 2013;44:47–50.
[15] Li X, Dong Z, Westwood A, Brown A, Zhang S, Brydson R, et al. Preparation of a titanium carbide coating on carbon fibre using a molten salt method. Carbon 2008;46:305–9.
[16] Tang Y, Deng Y, Zhang K, Liu L, Wu Y, Hu W. Improvement of interface between Al and short carbon fibres by α-Al_2O_3 coatings deposited by sol–gel technology. Ceram Int 2008;34:1787–90.
[17] Clement JP, Rack HJ, Wu KT, Spencer HG. Interfacial modification in metal matrix composites by the sol–gel process. Mater Manuf Process 1990;5:17–33.
[18] Chen R, Li X. A study of silica coatings on the surface of carbon or graphite fibre and the interface in a carbon magnesium composite. Compos Sci Technol 1993;49:357–62.
[19] Urena A, Rams J, Escalera MN, Sanchez M. Characterization of interfacial mechanical properties in carbon fibre/aluminium matrix composites by the nanoindentation technique. Compos Sci Technol 2005;65:2025–38.
[20] Shaw LL, Miracle DB. Effects of an interfacial region on the transverse behavior of metal–matrix composites-A finite element analysis. Acta Mater 1996;44:2043–55.
[21] Guo X, Derby B. Solid-state fabrication and interfaces of fiber reinforced metal matrix composites. Prog Mater Sci 1995;39:411–95.
[22] ASTM D3379-75. Standard test method for tensile strength and Young's modulus for high-modulus single-filament materials; 1989.
[23] Szlufarska I, Nakano A, Vashishta P. A crossover in the mechanical response of nanocrystalline ceramics. Science 2005;309:911–4.
[24] Xu X, Nishimura T, Hirosaki N, Xie RJ, Yamamoto Y, Tanaka H. Superplastic deformation of nano-sized silicon nitride ceramics. Acta Mater 2006;54:255–62.
[25] Bobylev SV, Mukherjee AK, Ovidko IA. Emission of partial dislocations from amorphous intergranular boundaries in deformed nanocrystalline ceramics. Scripta Mater 2009;60:36–9.
[26] Takeuchi A, Inoue A. Classification of bulk metallic glasses by atomic size difference, heat of mixing and period of constituent elements and its application to characterization of the main alloying element. Mater Trans 2005;46(12):2817–29.